ROYAL SOCIETY OF CHEMISTRY

Materials Horizons

COMMUNICATION

Search for Promising New Perovskite-Based Photovoltaic Absorbers: The Importance of Electronic Dimensionality†

Received 00th January 20xx, Accepted 00th January 20xx

Zewen Xiao,*a‡ Weiwei Meng,ab Jianbo Wang,b David B. Mitzi,*c and Yanfa Yan*a

DOI: 10.1039/x0xx00000x

www.rsc.org/

Searching for promising non-toxic and air-stable perovskite absorbers for solar cell applications has drawn extensive attention. Here, we show that a promising perovskite absorber should exhibit a high electronic dimesionality. Semiconductors that exhibit a high structural dimensionality, but a low electronic dimensionality have less promise as an absorber, due to barriers to isotropic current flow, enhanced electron/hole effective masses and fundamentally deeper defect states (more effective at causing recombination). Our concept accounts for the device performance of the perovskite-based solar cells reported in literature so far.

Introduction

Despite the rapid improvement in record power conversion efficiency (PCE) over the past six years, demonstrating the great potential of organic-inorganic lead (Pb) halide perovskite (ABX₃) solar cells, ¹⁻⁶ the commercialization of this emerging photovoltaic technology is still facing serious challenges due to cell instability against moisture and temperature and the inclusion of toxic Pb. Developing non- or low-toxicity and air stable halide perovskite-based solar cells has attracted extensive attention. ⁷⁻¹⁹ Theoretical studies have shown that the superior photovoltaic properties of Pb halide perovskite absorbers are partially attributed to their unique electronic features, including the Pb lone pair s orbital that causes strong Pb $5s^2 - 1$ $6p^6$ anti-bonding coupling, and the high perovskite symmetry. ²⁰⁻²² Therefore, searching for alternative Pb-free halide perovskites has focused on halide compounds

Conceptual insights:

A promising photovoltaic absorber should exhibit the following properties: high optical absorption, small carrier effective masses, and dominant defects that yield shallow levels. Structural dimensionality has been commonly used to explain the basis for desirable photovoltaic properties. Here, we introduce the concept of electronic dimensionality - the connectivity of the atomic-orbitals that comprise the lower conduction band and upper valence band. We show that electronic dimensionality accounts for photovoltaic properties much better than dimensionality, with high structural dimensionality providing the opportunity for (though not guaranteeing) high photovoltaic performance.

containing Ge^{2+} , Sn^{2+} , Sb^{3+} , and Bi^{3+} cations, which exhibit lone pair s orbitals.²³ These metal ions are known to form octahedra with halogen anions, which represent the required structural unit for forming perovskite structures and perovskite alternatives (also referred as non-perovskites).²⁴ Here, perovskites and perovskite alternatives refer to the structures consisting of corner-sharing and non-corner-sharing (e.g., edge-sharing, face-sharing, or even isolated) [BX₆] octahedra, respectively. These perovskites and perovskite alternatives can also be categorized by their structural dimensionality, i.e., 3D, 2D, 1D, 0D, 24 and even a fractional dimensionality, as will be defined later. A large number of Pbfree halide perovskites and perovskite alternatives with a wide range of bandgaps and different bandgap characteristics (direct vs indirect) have been reported. 11,13-15,25-36 So far, only Sn-based 3D perovskites have produced solar cells with reasonable PCEs;⁷⁻¹⁰ other Ge-, Bi-, and Sb-based perovskites and perovskite alternatives have not produced efficient devices. 11,12,28,34,36 Therefore, it is important to fully understand the trend of bandgaps and other photovoltaic properties of all reported materials and the causes for the inferior photovoltaic device performances.

Conventionally, structural dimensionality has been used as one metric to account for photovoltaic properties and device performances of absorbers. 34,37,38 This argument relies in part

^a Department of Physics and Astronomy, and Wright Center for Photovoltaic Innovation and Commercialization, The University of Toledo, Toledo, Ohio 43607, United States. Email: zwxiao@lucid.msl.titech.ac.jp, yanfa.yan@utoledo.edu

b. School of Physics and Technology, Center for Electron Microscopy, MOE Key Laboratory of Artificial Micro- and Nano-structures, and Institute for Advanced Studies, Wuhan 430072, China

^c Department of Mechanical Engineering and Materials Science, and Department of Chemistry, Duke University, Durham, North Carolina 27708, United States. Email: david.mitzi@duke.edu

 $^{^\}dagger$ Electronic Supplementary Information (ESI) available: Detailed data for Fig. 1. See DOI: 10.1039/x0xx00000x

[‡] Present address: Materials Research Center for Element Strategy, Tokyo Institute of Technology, Yokohama 226-8503, Japan

on the notion that current needs to effectively travel between contacts in a photovoltaic device before recombination and, given randomly oriented grains in an absorber film, the current path will be more direct if the transport properties are isotropic. While this notion is successful for most absorbers, it fails for some others. In this paper, we introduce a new concept, electronic dimensionality, which is the connectivity of the electronic orbitals that comprise the lower conduction band (LCB) and the upper valence band (UVB), to help understand photovoltaic properties such as bandgaps, carrier mobilities, defect levels and device performances of all reported Pb-free halide perovskites. While some perovskites are both structurally and electronically 3D, some perovskites are structurally 3D, but exhibit lower-dimensional electronic structures. We show that, to gain a full spectrum understanding of the photovoltaic properties and device performance, electronic dimensionality must be considered. Our results suggest that a promising photovoltaic absorber should have a high electronic dimensionality. Low electronic dimensionality implies that, at a minimum, films of the semiconductor must be grown with special crystallographic orientation to facilitate effective carrier transport. Our results provide critical guidance for the search for promising Pb-free halide perovskite photovoltaic absorbers and for fabricating efficient devices.

Results and Discussion

Perovskite and non-perovskite structural dimensionality has significant impact on the properties important for photovoltaic, including bandgap, carrier effective mass, optical absorption and, importantly, defect properties. Fig. 1 summarizes the experimental optical bandgaps and device performances of some metal iodide perovskites and nonperovskites. For lead-based iodide perovskites (red symbols), 3D $MAPbI_3$ (MA = CH_3NH_3), $FAPbI_3$, (FA = $HC(NH_2)_2$), and CsPbI₃, have bandgaps of 1.52 eV, ²⁵ 1.48 eV, ²⁵ and 1.67 eV, ²⁵ respectively, which are suitable for single-junction solar cell applications. Layered perovskites can be structurally derived from their 3D analogues by slicing along specific crystallographic planes. 24,39,40 The most common structure is the (100)-oriented type with the general chemical formula of $(RNH_3)_2(MA)_{n-1}B_nX_{3n+1}$ (n is the number of [PbI₆] octahedra layers), which is obtained by stacking n perovskite layers along the (100) direction of the parent 3D structure, separated by the long spacer ammonium cations RNH₃⁺. The thickness of the parent octahedra layers can be controlled by varying the molar ratio between the large organic cation and the parent perovskite precursors. Here, the structural dimensionalities of the single-layered (n = 1) and the infinite-layered $(n = \infty)$ perovskites are 2 and 3, respectively. Therefore, the dimensionality of a multi-layered perovskite can semiquantitatively be expressed as 3 - 1/n, i.e., with values between 2 and 3 (see the horizontal axis of Fig. 1a).

The bandgap of a 2D single-layered perovskite $(RNH_3)_2Pbl_4$ can be tuned by controlling factors such as the interlayer spacing (i.e., the length of the spacing cation RNH_3) and the

structural distortion within the perovskite layer, 41 because increasing the interlayer spacing and the degree of distortion can decrease the band widths, particularly, of the VBM and the CBM. The bandgap of $(RNH_3)_2PbI_4$ is 2.57 eV, ⁴² 2.70 eV, ⁴³ 2.82 eV, 44 and 2.88 eV, 45 when the spacing cation is $C_6H_5(CH_2)_2NH_3$ (PEA), $C_6H_{13}NH_3$, $C_9H_{19}NH_3$, and $C_{12}H_{25}NH_3$, respectively. The increasing bandgap trend should be partially attributed to the increasing interlayer spacing caused by the increasing length of the organic molecular cations. On the other hand, 2D singlelayered perovskite (CH₃NH₃)₂Pb(SCN)₂I₂, which consists of SCN⁻ anion-terminated octahedra layers, has a relatively small bandgap of 2.1–2.3 eV, 46,47 primarily, because of the small interlayer spacing. The bandgaps of the multi-layered $(PEA)_2(MA)_{n-1}Pb_nI_{3n+1}$ perovskite family members are shown in Fig. 1a. As n increases to 2 and 3, the bandgap decreases to 2.32 eV^{42} and 2.1 eV^{37} As *n* further increases to 6 and 10, the structural dimensionality becomes closer to 3 and, correspondingly, the bandgap becomes close to that of 3D MAPbl₃ $(n = \infty)$. ⁴⁸ The similar *n* dependence of bandgap is also observed in other families of layered perovskites including $(C_6H_{13}NH_3)_2(CH_3NH_3)_{n-1}Pb_nI_{3n+1}$,⁴³ $(C_3H_7NH_3)_2(CH_3NH_3)_{n-1}$ $_{1}\text{Pb}_{n}\text{I}_{3n+1}$, 49 and $(C_4H_9NH_3)_2(CH_3NH_3)_{n-1}Pb_nI_{3n+1}$. (NH₂C(I)=NH₂)₃PbI₅ is a structurally 1D perovskite consists of corner-sharing [PbI₆] chain, and has a large bandgap of 3.18 eV.⁵¹ (CH₃NH₃)₄Pbl₆·2H₂O consists of isolated [Pbl₆] octahedra and should be considered as a OD non-perovskite because the [PbI₆] octahedra lose the "corner-sharing" feature. The bandgap of (MA)₄PbI₆·2H₂O is as large as 3.87 eV.⁴⁴ δ-CsPbI₃ consists of double-chains of non-corner-sharing [PbI₆] octahedra and has a structural dimensionality of 1.5 (i.e., 2 -1/2 for double-chains). The 1.5 D δ -CsPbI $_3$ has a much larger bandgap (3.14 eV⁵²) than the cubic 3D CsPbI₃ (1.67 eV), although they are polymorphs. Based on these literature results, we conclude that the general trend is that the bandgap increases with decreasing of structural dimensionality. As seen in Fig. 1a, the Sn-based halides exhibit the same structural dimensionality dependence of the bandgap. 3D MASnI₃, FASnI₃, and CsSnI₃ have bandgaps of 1.20 eV, ²⁵ 1.41 eV, ²⁵ and 1.30 eV, 25 respectively. 2D (PEA)₂SnI₄, 1D (NH₂C(I)=NH₂)₃SnI₅, and OD (MA)₄SnI₆·2H₂O, have bandgaps of 2.19 eV, ⁵³ 3.02 eV, ⁴⁴ 3.54 eV, 44 respectively. The bandgaps of the Sn-based halides are lower than that of Pb-based counterparts, primarily because of the higher energy levels of Sn 5s orbitals as compared to Pb 6s orbitals.

Recently, trivalent Bi³⁺ and Sb³⁺ also have been used to replace Pb to form Pb-free halide perovskites. $^{11-14,28-30,36,54-57}$ However, the resulting compounds expressed by the general chemical formula of $A_3^*B_2^{3+}\chi_9^-$ have to crystallize into lower-dimensional structures to keep charge neutrality. There are two typical polymorphs for $A_3B_2X_9$. One is a (111)-oriented bilayered perovskite structure, and the corresponding chemical formula can be expressed as $A_3\Box B_2X_9$ (\Box indicates B vacancy), where each one \Box layer and two B-atom layers are alternatively stacked along the <111> direction of the parent perovskite structure. 24,28 These bi-layered $A_3B_2X_9$ perovskites have structural dimensionality of 2.5 (i.e., 3-1/2 for n=2) and the bandgaps are on the order of 2 eV (e.g., (NH₄)₃Bi₂l₉: 2.04

eV; 13 Rb₃Bi₂I₉: 2.1 eV; 14 and Cs₃Sb₂I₉: 2.05 eV 28). The other is non-perovskite phase $A_3B_2X_9$ consisting of A^+ cations and isolated $[B_2X_9]^{3-}$ units (each $[B_2X_9]$ unit consists of two facesharing [BX₆] octahedra). Here, the structural dimensionality of $A_3^{\dagger}[B_2X_9]^{3-}$ is considered as 0.5 (i.e., 1-1/2 for bioctahedra), higher than those consisting of isolated [BX₆] octahedra (i.e., 0D). Because of the further lower crystal dimensionality, the A₃B₂X₉ non-perovskites have much larger bandgaps than their bi-layered perovskite counterparts. For example, Cs₃Bi₂I₉ and (MA)₃Bi₂I₉ non-perovskites have bandgaps of 2.86 eV⁵⁸ and 2.9 eV,³⁶ respectively. However, some groups reported much smaller bandgaps for Cs₃Bi₂I₉ and (MA)₃Bi₂I₉ nonperovskites. 11,12,56,57 It is known that low-dimensional semiconductors generally exhibit an exciton band below the absorption edge. However, these groups determined the bandgaps from the exciton band, rather than the fundamental absorption band edges, leading to much underestimated bandgap values.

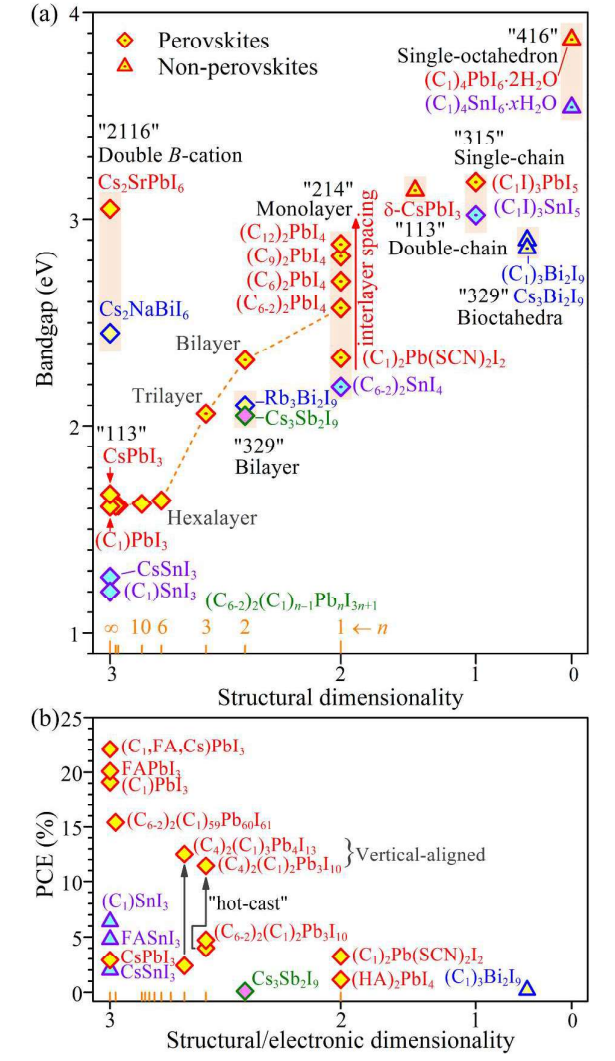


Fig. 1 (a) Experimental bandgaps of some iodide perovskites (diamond symbols) and non-perovskites (triangle symbols) as a function of crystal dimensionality. For the dot-center symbols, optical bandgaps were determined by excluding the exciton band

at low temperature. The structural dimensionality of an n-layered perovskite is defined as 3-1/n. Similarly, the structural dimensionality of the compounds that comprise double-[Pbl₆]-chains is qualitatively defined as 1.5, and that for bioctahedrabased compounds as 0.5. (b) Highest recorded efficiencies for some iodide perovskite and non-perovskite absorber materials. " C_n " indicates $C_nH_{2n+1}NH_3$, " C_{6-2} " indicates $C_6H_5(CH_2)_2NH_3$, " C_1I " indicates $NH_2C(I)=NH_2$, "FA" indicates $HC(NH_2)_2$, and "HA" indicates $C_5N_3H_{11}$. The detailed data for Fig. 1a and b are given in Table S1 and S2 in the Supporting Information, respectively.

Most of the reported bandgap values of the materials shown in Fig. 1a correlate well with the structural dimensionality. We show that the underlying reason is that these materials have the same structural and electronic dimensionality. It is their electronic dimensionalities that determine the bandgap values. To help understand the effects of structural and electronic dimensionality on the photovoltaic properties of perovskite materials, we show DFT calculated photovoltaic properties for prototype perovskite materials consisting of the same elements of Cs, Pb, and I, but different crystal dimensionalities, i.e., 3D CsPbI₃, 2D Cs₂PbI₄, 1D Cs3PbI₅, and 0D Cs₄PbI₆, which consist of 3D network, 2D monolayers and 1D single-chains of [PbI₆] octahedra, and isolated [PbI₆] octahedra, respectively (see Fig. 2a). Fig. 2b and c show the calculated band structures and optical absorption spectra of these materials, respectively. CsPbI₃ exhibits a direct bandgap at the R point. The valence band maximum (VBM) consists of I 5p - Pb 6s antibonding states, while the conduction band minimum (CBM) is composed mainly of Pb 6p states. It is important to note that the CBM- and VBM-deriving Pb 6s, 6p, and I 5p atomic orbitals connect 3-dimentionally, exhibiting a 3D electronic dimensionality. It is because of this 3D electronic dimensionality, both the VBM and CBM are dispersive along all directions, leading to mobile charge carries along all directions. Due to the p-p transition, CsPbI₃ exhibits high and isotropic optical absorption. These results are consistent with the wellestablished literature on 3D halide perovskites. 59,60

2D Cs₂PbI₄ has a direct bandgap of 1.90 eV at the M point (see the second panel of Fig. 2b), which is much larger than that of 3D CsPbI₃ (1.48 eV). The calculated band structure reveals dispersive characters for the LCB and UVB for the 2D Cs₂PbI₄ perovskite along the M-X and A-R directions, which are parallel to the [PbI₆] octahedra layers, indicating that the carriers are mobile within the layers. This is because this 2D perovskite also exhibits a 2D electronic dimensionality, i.e., the CBM- and VBM-deriving Pb 6s, 6p, and I 5p atomic orbitals connect in the octahedra layers. However, there is almost no orbital connection along the direction perpendicular to the octahedra layers due to the van der Waals interaction between the layers. As a result, there is almost no dispersion for the states near the CBM and VBM along the M-A direction (i.e., [001]). Therefore, the charge carriers exhibit almost infinite effective masses along the T-R direction and are immobile across the layers; that is, the charge carriers are confined within the 2D layers. Also, because of the 2D electronic dimensionality associated with the layered

structure, the optical absorption coefficients (α) of the 2D Cs₂PbI₄ perovskite exhibit strongly anisotropic character (see the second panel of Fig. 2c). The α along the [001] direction crossing the layers (blue dotted line) is much weaker for low energy photons than those along the [100] and [010] directions parallel to the layers (black solid and red dashed lines, respectively). There is no noticeable absorption until around 0.3 eV above the bandgap along the [100] direction. However, because of the p-p transition feature, Cs₂PbI₄ still exhibits a high total absorption coefficient and may still be used as the top cell in tandem solar cell applications. These results are generally consistent with our previous study on the 2D perovskite (CH₃NH₃)₂Pb(SCN)₂I₂. ⁴⁶ Due to the 2D electronic dimensionality, both VB and CB have slightly narrower band widths, leading to a lower VBM, a higher CBM and, therefore, a larger bandgap as compared to its 3D counterpart CsPbl₃.⁶¹⁻

1D Cs₃Pbl₅ exhibits an indirect bandgap of 2.80 eV with the VBM at the T point and the CBM at the Γ point. The VBM and the CBM are dispersive only along the T-R and the Γ-X directions, respectively, which are parallel to the [PbI₆] octahedra chains. This is because the CBM- and VBM-deriving Pb 6s, 6p, and I 5p atomic orbitals connect only along the octahedra chains, but do not connect along the directions perpendicular to the chains. Therefore, this structurally 1D material also exhibits a 1D electronic dimensionality. The bands along the directions perpendicular to the chains (i.e., U-X, Γ-T, and R-S) are fairly non-dispersive, indicating poor carrier mobility across the chains. The CB and VB are much narrower, responsible for the increased bandgap as compared to its 3D and 2D counterparts. The optical absorption coefficients of Cs₃Pbl₅ are anisotropic. The absorptions along the directions perpendicular to the chains (the blue dotted and the red dashed lines) are much weaker than that along the chain direction (black solid line) for photons in the region of about 1 eV above the bandgap. 0D Cs₄PbI₆ exhibits a direct bandgap of 3.44 eV at the Γ point. The VBM and the CBM are non-dispersive along all directions because of the isolation of the [PbI₆] octahedra, in which the CBM- and VBM-deriving Pb 6s, 6p, and I 5p atomic orbitals do not connect. Therefore, this structurally OD perovskite also exhibits a OD electronic dimensionality, which is fundamentally responsible for the large bandgap. Based on these results, 1D and 0D perovskites are not promising photovoltaic absorbers. The results explain why all 0D and 1D perovskites shown in the upper right corner of Fig. 1 exhibit high bandgap values.

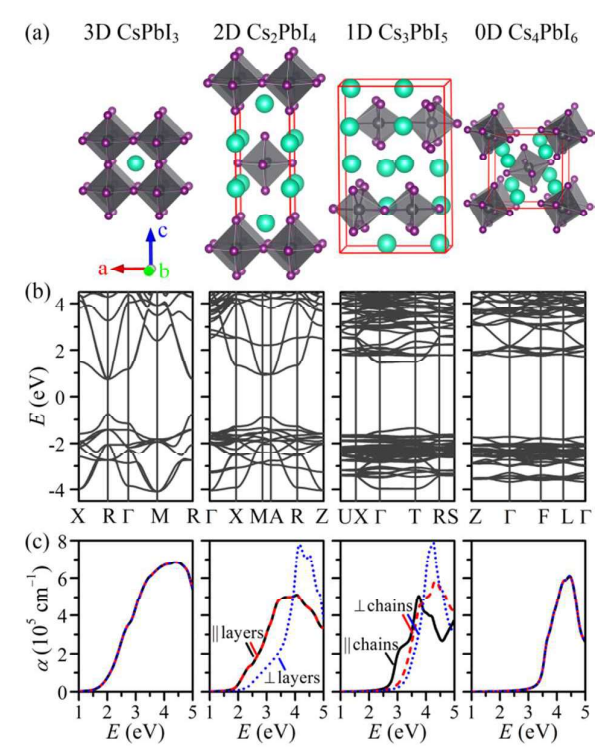


Fig. 2 (a) Hypothetical model crystal structures of CsPbl₃ (cubic, Pm-3m), ⁶⁴ Cs₂Pbl₄ (following K₂NiF₄, ⁶⁵ tetragonal, I4/mmm), Cs₃Pbl₅ (following [CH₃SC(NH₃)₂]₃Snl₅, ⁶⁶ orthorhombic, Pnam), and Cs₄Pbl₆ (following Cs₄PbBr₆, ⁶⁷ rhombohedral, R-3c). (b) Calculated band structures and optical absorption coefficients of model systems CsPbl₃, Cs₂Pbl₄, Cs₃Pbl₅, and Cs₄Pbl₆.

Recently, layered (2D) lead iodide-based perovskites have attracted much attention for solar cell application because of their higher environmental stability and film quality. Among the 2D single-layered perovskites, 50,68-70 (CH₃NH₃)₂Pb(SCN)₂I₂ has shown the highest PEC of 3.23%, 70 which is still much lower than the values attainable for the 3D perovskites. An obvious way to enhance the PCE is to increase the electronic/structural dimensionality by increasing the layer number n. ^{37,48} To illustrate this, we examined the photovoltaicrelevant properties of a family of $Cs_{n+1}Pb_nI_{3n+1}$ layered perovskites by DFT calculations. Fig. 3a shows the crystal structure of the n = 4 member. Fig. 3b shows the calculated bandgaps of the $Cs_{n+1}Pb_nI_{3n+2}$ layered perovskite family. The calculated bandgap for the n=1 member is 1.90 eV. As nincreases to 10, the bandgap steadily decreases to 1.51 eV, which is fairly close to that of the 3D counterpart $(n = \infty)$ CsPbI₃ (1.48 eV), explaining the experimental trend shown in Fig. 1a. Fig. 3c shows the effective carrier masses calculated from the band structures (Fig. 3d). It is important to note that the electronic dimensionality is the same as the structural dimensionality for this system. The in-plane effective masses of both electron and hole (e.g., along the M-X direction) decrease as n increases. However, increasing n up to 10 cannot remove the anisotropic nature of the carrier transport properties. The out-of-plane effective electron mass (i.e., along

the M–A direction) also decreases as *n* increases; however, the hole mass remains almost infinite for the layered perovskites (at least for n = 1-10). For the optical properties, increasing the n value significantly enhances the optical absorption, because of the decreased bandgap and reduced anisotropy in the optical response (Fig. 3e). Therefore, the trend of the electronic and optical properties and carrier mobility can be fundamentally understood by the structural and electronic dimensionality. Smith et al. used the n = 3 member of (C_{6} - $_{2})_{2}(C_{2})_{n-1}Pb_{n}I_{3n+1}$ layered perovskite family as absorbers in solar cells, which achieved a PEC of 4.73%.³⁷ Moreover, as is evident from the structure, 46 these layered perovskites should be grown with the layers perpendicular to the substrates to achieve better photovoltaic properties, including higher carrier mobility and higher optical absorption, and thus higher PECs. Most recently, Tsai et al. 71 have successfully obtained verticalaligned $(BA)_2(MA)_2Pb_3I_{10}$ and $(BA)_2(MA)_3Pb_4I_{13}$ films via the "hot-casting" method. The best PECs of their solar cells reached to 11.44% and 12.52%, respectively, which are much higher than those for the non-vertical-aligned counterparts (4.02% and 2.39%, respectively), 50 but still lower than those for the 3D lead iodide perovskites, presumably because of the properties associated with the lower electronic dimensionality of these layered perovskite materials, e.g., larger bandgaps.

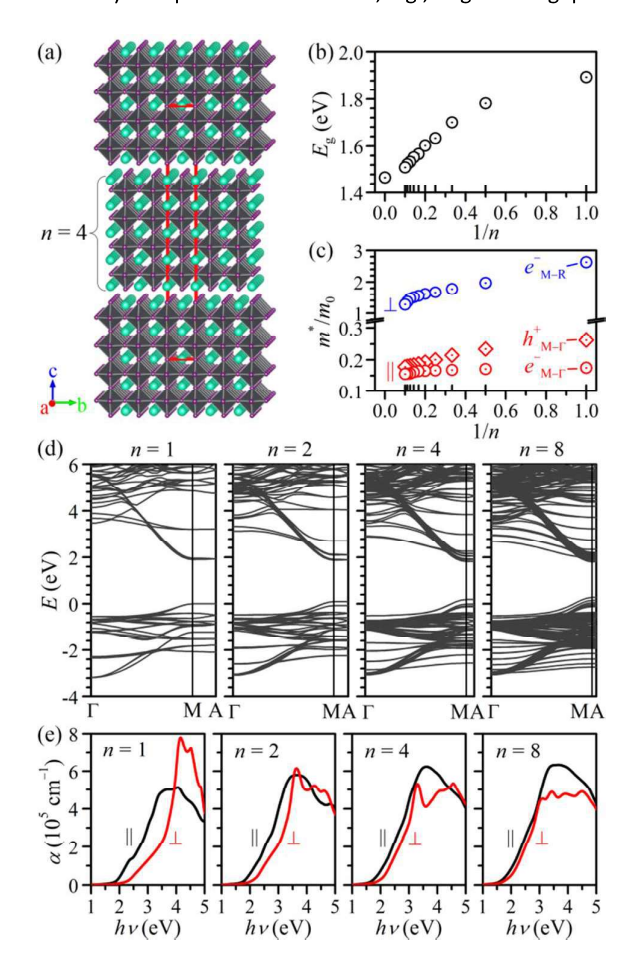


Fig. 3 (a) Crystal structure of the n=4 member of the hypothetical $Cs_{n+1}Pb_n|_{3n+1}$ layered perovskite family (tetragonal, space group I4/mmm). (b) Calculated bandgaps and (c) in-plane (red) and out-of-plane effective electron (the circles symbols) and hole (the diamond symbol) masses of the $Cs_{n+1}Pb_n|_{3n+2}$ layered perovskite family. The out-of-plane hole masses of these layered perovskites are almost infinite and are not shown. (d) Band structure and (e) absorption coefficient of the n=1,2,4,8 members of the $Cs_{n+1}Pb_n|_{3n+2}$ layered perovskite family.

The above materials exhibit the same structural and electronic dimensionality. Therefore, the bandgap trend, optical properties, and device performance can be explained well by the structural dimensionality. However, there are perovskites exhibiting electronic dimensionalities lower than their structural dimensionalities. For these perovskites, the trend of bandgap and optical properties can no longer be explained solely by the structural dimensionality; the electronic dimensionality must be considered. There are two major causes for lower electronic dimensionality: structural or chemical deviation.

The structural deviation is related to the rotation and/or distortion of [BX₆] octahedra. It is known that the bandgap of a perovskite can be affected by the structural distortion. 41,72,73 Here, we show that the trend of the changes of photovoltaic properties caused by structural distortion can be qualitatively understood by the change of the electronic dimensionality. To understand this, we choose ideal model 3D CsPbI₃ and 2D Cs2PbI₄ perovskites as examples, in which all the Pb-I-Pb bond angles are 180°. For simplicity, we only change the in-plane Pb-I-Pb bond angle (denoted as θ in Fig. 4a) but fix the out-ofplane Pb-I-Pb bond angle. 41 In addition, all Pb-I bond lengths are the same (no distortions introduced to the octahedra). Fig. 4b summarizes the calculated bandgaps as a function of the inplane Pb-I-Pb bond angle θ . As the θ decreases from 180° to 136.4°, the bandgap of 3D CsPbl₃ increases slowly from to 1.48 eV to 1.66 eV, while the bandgap of 2D Cs₂PbI₄ increases rapidly from 1.89 eV to 2.51 eV. Fig. 4c shows the calculated band structures, and Fig. 4e and f show the VBM- and CBMassociated charge density maps on the (001) plane (i.e., the ab plane). For the ideal 3D CsPbI₃ perovskite (see the first panels of Fig. 4c, d, and e), the VBM is composed of strongly-coupled I 5p and Pb 6s orbitals, while the CBM mainly consists of Pb 6p orbitals, among which, Pb 6px, 6pv and 6pz orbitals contribute equally to the CBM. The rotation of the [PbI₆] octahedra does not change the structural dimensionality, i.e., 3D, but it does lower the connectivity of I 5p and Pb 6s orbitals and the connectivity (overlap) of Pb $6p_x$, and $6p_y$ orbitals, leading to a reduced electronic dimensionality. For the θ = 136.4° CsPbI $_3$ (see the second panels of Fig. 4c, d, and e), the in-plane I atoms are off the centers of the line of two-neighboring Pb atoms, which reduces the in-plane orbital overlap between Pb and I atoms. On the one hand, the Pb 6s-I 5p coupling is significantly weakened, which makes the UVB narrower and thus the VBM lower and less dispersive. On the other hand, because of the structural distortion, the Pb 6px- and 6pvderived conduction bands also become narrower and

contribute little to the LCB. The Pb 6p₂-derived bands are less affected by the in-plane structural distortion and are slightly narrowed, making the VBM slightly higher in energy. As a result, the distortion-induced bandgap widening for CsPbi₃ is relatively small (Fig. 3b). It should be noted that the structural distortion slightly reduces the connectivity of the atomicorbitals that comprise the LCB and UVB; therefore, the electronic dimensionality is slightly less than 3, though it is difficult to assign an exact value. This connection between structural distortion and electronic structure explains the bandgap variations for lead halide perovskites with different structures such as the cubic and tetragonal phases. ^{25,74,75}

For the ideal 2D Cs₂PbI₄ perovskite (see the third panels of Fig. 4c, d, and e), the electronic properties have been discussed above. Here, it should be noted that the LCB consists mainly of only Pb $6p_x$ and $6p_y$ orbitals. The Pb $6p_z$ orbitals contribute very little to the LCB, because the Pb 6p₂-derived bands are largely narrowed due to the 2D structure. 61 For the $\theta = 136.4^{\circ} \text{ Cs}_{2}\text{Pbl}_{4}$ (see the forth panels of Fig. 4c, d, and e), again, the VBM becomes lower and less dispersive, because the Pb 6s-I 5p coupling is weakened by the structural distortion. Additionally, the Pb 6px- and 6pv-derived bands, which account for the CBM, are narrowed due to the structural distortion, effectively raising the CBM level. As a result, the inplane-distortion-induced bandgap widening of structurally-2D Cs₂PbI₄ is much larger than that for structurally-3D CsPbI₃. Therefore, structural distortion can significantly affect the bandgaps of 2D layered perovskites, explaining the "scattered" nature of bandgaps for 2D layered perovskites. 41 The electronic dimensionality of these distorted layered perovskites should be considered lower than 2, but it is difficult to define it quantitatively.

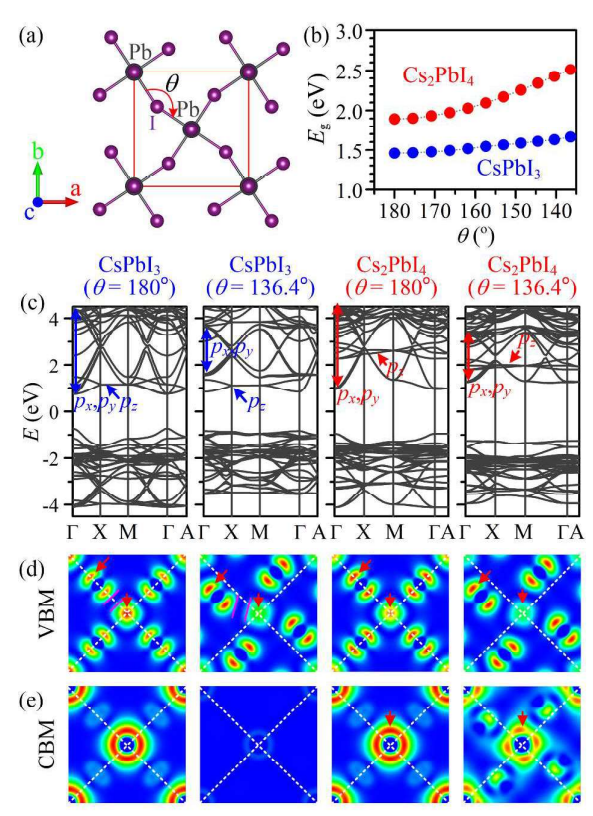


Fig. 4 (a) Schematic of Pb–I–Pb bond distortion in the ab plane of $V2\times V2$ -cells of CsPbI₃ and Cs₂PbI₄ perovskites. (b) Calculated bandgaps of CsPbI₃ and Cs₂PbI₄ perovskites as a function of the inplane Pb–I–Pb bond angle θ . (c) Calculated band structures and (d) VBM- and (e) CBM-associated charge density maps on the (001) plane for ideal undistorted (θ = 180°) and distorted (θ = 136.4°) CsPbI₃ and Cs₂PbI₄ perovskites.

To help understand how chemical deviations can lower the electronic dimensionality as compared to structural dimensionality, we calculate the band structures of two prototype double perovskites Cs₂SrPbI₆ and Cs₂NaBiI₆, whose bandgap values are shown in the upper left-hand corner of Fig. 1a. These double perovskites are structurally 3D, but they have bandgaps significantly larger than the 3D single-B-cation perovskites, e.g., CsPbl₃, MAPbl₃, FAPbl₃. Fig. 5a shows a 2 × 2 × 2 supercell of the 3D CsPbI₃ perovskite, which can be regarded as a nominal "double" perovskite of Cs₂PbPbI₆, which is isostructural to $Cs_2AgBiBr_6$ (i.e., in the Fm-3m space group). We compare the DFT calculated photovoltaic properties of this nominal and a real double perovskite such as Cs₂SrPbI₆ (Fig. 5b). It is seen that Cs₂SrPbI₆ is composed of a 3D octahedra network of alternatively-corner-shared [SrI₆] and [PbI₆] octahedra and, therefore, exhibits a 3D structural dimensionality. However, it should be noted that the [PbI₆] octahedra are isolated by the [SrI₆] analogues.

Fig. 5c and d show the calculated band structures for Cs_2PbPbI_6 and Cs_2SrPbI_6 . It is seen that Cs_2PbPbI_6 exhibits a direct bandgap with both VBM and CBM located at the Γ point. The VBM consists of I 5p–Pb 6s antibonding states while the

CBM consists of Pb 6p-I 5p antibonding states (see the calculated charge density maps of the VBM and CBM, as shown in Fig. 5e and g, respectively). It should be noted that both the VBM and the CBM derived from the 3D cornersharing [PbI₆] octahedra are relatively dispersive, leading to reasonably good carrier transport properties. For the double perovskite Cs₂SrPbI₆, the calculated band structure exhibits an indirect bandgap of 3.05 eV with the VBM at the Γ point and the CBM at the L point. This bandgap value is much larger than that of 3D CsPbI₃ (1.48 eV), but is comparable to the calculated bandgap of OD Cs₄PbI₆ (3.44 eV). The VBM and CBM of Cs₂SrPbI₆ consist of I 5p-Pb 6s antibonding states and the Pb 6p-I 5p antibonding states, respectively, similar to Cs₂PbPbI₆. However, the [Srl₆] octahedra do not make contribution to the CBM and VBM. Therefore, the CBM- and VBM-deriving Pb 6s, 6p, and I 5p atomic orbitals ([PbI₆] octahedra) do not connect (see Fig. 5f and h), giving the double perovskite Cs₂SrPbI₆ effectively a 0D electronic dimensionality. Therefore, the lower CB and upper VB bands are fairly non-dispersive, resembling the electronic properties of the OD perovskites.

The OD electronic dimensionality has significant effects on the defect properties of the absorbers. Figs. 4i and j show the calculated transition levels of vacancies in Cs2PbPbI6 and Cs₂SrPbI₆, respectively. For Cs₂PbPbI₆, the (0/1–) transition of V_{Cs} and the (0/1–) and (1–/2–) transitions of V_{Pb} are below the VBM and therefore are inert. For V_I, the (0/1+) transition is located at 0.28 eV below the CBM, while the (0/1–) transition is above the CBM. These results indicate that Cs₂PbPbI₆ exhibits good defect tolerance, consistent with previous reports on 3D CH₃NH₃PbI₃.^{60,77,78} In contrast, Cs₂SrPbI₆ systematically exhibits deeper defect transition levels than Cs_2PbPbI_6 . The (0/1–) transition of V_{Cs} is located at 0.17 eV above the VBM. The (0/1-) and (1-/2-) transitions are located at 0.15 eV and 0.40 eV above the VBM, respectively. The (0/1+) and (0/1-) transitions are located at 0.50 eV and 0.39 eV below the CBM, respectively. These deep defects may act as electron traps, hole traps, and/or recombination centres, which deteriorate the device performance. The deep nature of the defects in Cs₂SrPbI₆ can be qualitatively explained by the 0D electronic dimensionality, causing lower VBM and higher CBM than its 3D counterpart Cs₂PbPbI₆, which is similar to the case of the 2D (CH₃NH₃)₂Pb(SCN)₂I₂ perovskite.⁶³

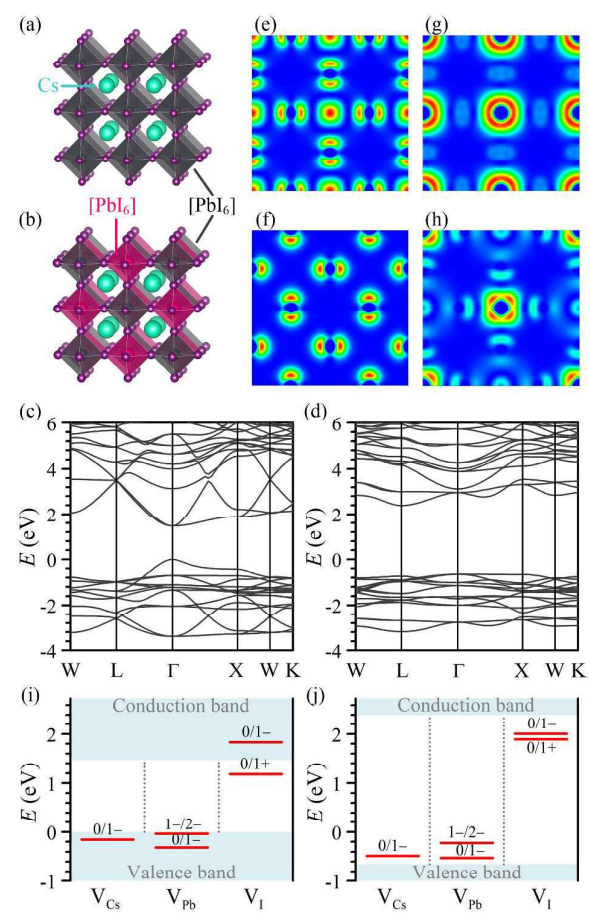


Fig. 5 (a,b) Crystal structures, (c,d) band structures, (e,f) VBM- and (g,h) CBM-associated charge density maps on the (100) plane, (i,j) calculated defect transition levels of (a,c,e,g,i) Cs₂Pb₂I₆ and (b,d,f,h,j) Cs₂SrPbI₆. In Figs. e,d,l,j, the relative VBM and CBM positions of Cs₂PbPbI₆ and Cs₂SrPbI₆ are aligned by matching core levels.

The electronic dimensionality can also explain the photovoltaic-relevant properties of Bi-based double B-cation perovskites such as Cs_2AgBiX_6 (X = Br and CI), 15,31,79,80 and (MA)₂KBiCl₆,³² which have recently attracted significant attention. The bromides Cs₂AgBiBr₆ , (MA)₂TlBiBr₆, ³³ and chlorides Cs₂AgBiCl₆ and (MA)₂KBiCl₆ exhibit indirect bandgaps of 1.95 eV, 15 2.77 eV, 31 >3.04 eV, 32 respectively. Cs₂AgBil₆ is expected to have a smaller bandgap; however, it cannot be readily synthesized because of the negative decomposition energy $(Cs_2AgBil_6 \rightarrow \%CsAg_2l_3 + \%Cs_3Ag_2l_9, -0.47 \text{ eV})$. 81 Like the prototype compounds Cs₂SrPbI₆ and Cs₂NaBiI₆, the Ag- and Bibased double perovskites Cs2AgBiX6 are electronically OD, although structurally 3D. Taking Cs₂AgBiBr₆ as an example, the DFT calculated band structure shows that the VBM is mainly derived from Ag 4d-Br 5p anti-bonding states, whereas the CBM is mainly derived from Bi 6p-Br 4p antibonding states.⁸¹ However, as Bi 6s orbitals do not contribute to the VBM due to their lower energy position as compared to the Ag 4d orbitals, the VBM-deriving Ag 4d and Br 5p orbitals cannot connect in three dimensions because the [AgBr₆] octahedra are isolated

by the adjacent [BiBr₆] octahedra. Similarly, the CBM-deriving Bi 6p and Br 5p orbitals cannot connect 3 dimensionally because of the isolated [BiBr₆] octahedra. As a result, Cs₂AgBiBr₆ has an indirect bandgap because of the mismatch in angular momentum of the VBM- and CBM-deriving atomic orbitals, 82 and large carrier effective masses along some directions because of the OD electronic dimensionality. Moreover, the defect calculations suggest that V_{Bi} and Ag_{Bi} are the dominant defects, which, however, show deep chargestate transition levels.⁸¹ Based on this understanding, double perovskites such as Cs₂AgBiBr₆ do not exhibit promising photovoltaic properties comparable to MAPbI₃. More recently, on the other hand, based on DFT calculations, Savory et al. reported that replacing Ag with In or TI can yield good photovoltaic-relevant properties.⁸² Deng et al. has synthesized (MA)₂TIBiBr₆,³³ and confirmed the direct character of the bandgap (around 2.0 eV). Based on our electronic dimensionality concept, the In-/TI- and Bi-based double perovskites are electronically 3D, because In/TI has similar contribution to the LCB and UVB, leading to a 3D connectivity of atomic-orbitals. However, these perovskites exhibit intrinsic thermodynamic instability and the narrow-bandgap iodide analogues have not been successfully synthesized. So far, there have been no reports on working solar cells based on these Sb- and/or Bi-containing double perovskites.

As a lead-free and air-stable perovskite variant, Cs₂SnI₆ has much attention also attracted for solar cell application. $^{16,19,27,83-87}$ $\mathrm{Cs_2Snl_6}$ also crystallizes in the the $\mathit{Fm}-$ 3m space group and can be regarded as a vacancy-ordered double perovskite, expressed as $Cs_2\square SnI_6$ (\square indicates Snvacancy (V_{Sn})), where Sn atoms and vacancies adopt a rocksalt-type arrangement. Both the VBM and the CBM of Cs₂SnI₆ are derived from the isolated [SnI₆] octahedra; therefore, Cs₂SnI₆ is electronically OD. Because of the fairly localized VBM, Cs₂SnI₆ exhibits a large hole effective mass and thus a low hole mobility. 19,85 In addition, the dominant defects (i.e., V_I and Sn_i) in Cs₂SnI₆ exhibit deep charge-state transition levels, which may act as electron and hole trap centers,86 and/or recombination centers, deteriorating the device performances. Currently, the solar cells based on Cs₂SnI₆ absorbers have achieved only about 1% PCE.87

The electronic dimensionality can also account for the performances of perovskites and perovskitealternatives listed in Fig. 1b. When the structural dimensionality decreases to $2 \le 3-1/n < 3$, the absorbers become layered perovskites, such as $(C_6H_{13}NH_3)_2(CH_3NH_3)_{n-1}$ $(C_3H_7NH_3)_2(CH_3NH_3)_{n-1}Pb_nI_{3n+1}$ $(C_4H_9NH_3)_2(CH_3NH_3)_{n\cdot 1}Pb_nI_{3n+1}.^{50}.\quad Though\quad these\quad perovskites$ exhibit reasonable bandgaps and optical absorption characteristics, device performances based on films with randomly-oriented grains are much lower compared to the 3D MAPbl₃ and FAPbl₃ perovskites. This is because the photogenerated charges cannot effectively travel across the gap between the inorganic layers, due to the lower electronic dimensionality. To enhance the PCEs, these layered perovskites must be grown such that the interlayer direction within the crystallites is perpendicular to the substrate surface

to facilitate charge collection, which has been demonstrated by Tsai *et al.*⁷¹ With further decrease of the structural and electronic dimensionality, the perovskites and perovskite-alternatives, such as Cs₃Sb₂l₉, (MA)₂Pb(SCN)₂l₂, (HA)₂Pbl₄, Cs₃Bi₂l₉, and (MA)₃Bi₂l₉, exhibit even poorer device performances (Fig. 1b). Such poor performance cannot be explained solely by their relatively wide bandgap, because these cells show very poor open-circuit voltages, relative to the large bandgaps, indicating strong non-radiative recombination in the absorbers. The large averaged effective masses and deep defect levels caused by the low electronic dimensionalities are likely the fundamental reasons for the strong non-radiative recombination.

It should be noted that having a 3D electronic structure with appropriate band gap does not guarantee good photovoltaic properties. FASnl₃, MASnl₃, and CsSnl₃ are all structurally and electronically 3D. They exhibit suitable bandgaps for single-junction solar cell applications, but the PCEs of solar cells based on these absorbers are rather poor as compared to MAPbl₃ and FAPbl₃ based solar cells. For 3D Sn-based perovskites, the facile oxidization of Sn²⁺ to Sn⁴⁺ causes a high density of Sn vacancies, leading to significant charge recombination and poor device performance.^{7,88} The black CsPbl₃ phase is also structurally and electronically 3D, but it does not produce efficient solar cells.^{89,90} This is because CsPbl₃ is not stable because of the relatively small Cs⁺ ions, which lead to a too small structural tolerance factor.⁹¹

Conclusions

We show that, to gain a full spectrum understanding of the photovoltaic properties and device performance of an absorber, the electronic dimensionality should be considered. The commonly used structural dimensionality explains the photovoltaic properties of some absorbers, but fails to account for others. This is because the structural and electronic dimensionalities are the same for some semiconductors, but different for others. We show that some double perovskites, such as the Ag- and Bi-containing halide double perovskites are structurally 3D, but electronically 0D. High electronic dimensionality is preferred for high-performance photovoltaic materials. The electronic dimensionality can account for many of the trends observed for photovoltaic properties and device performances of perovskite and perovskite alternatives reported in literature. Our results provide critical guidance for searching for Pb-free halide perovskite photovoltaic absorbers and for fabricating efficient devices.

Computational Method

Density functional theory (DFT) calculations were performed using the projector-augmented wave (PAW) method, as implemented in the VASP code. The plane-wave cutoff energy was set to 300.0 eV. Γ -centered k-meshes with k-spacing of 0.3 Å^{-1} were employed for sampling the Brillouin zones. The general gradient approximation (GGA) Perdew—

Burke–Ernzerhof (PBE)⁹³ functional was used for exchange-correlation. Prior to the electronic structure calculations, the structure was fully relaxed and considered to be converged when the total force on each atom was <0.01 eV Å⁻¹. Total-energy defect calculations were performed for CsPbI₃ and Cs₂SrPbI₆ a 320-atoms supercell and the Γ -only k-mesh. The atomic positions of the defect structures were relaxed until the total force on each atom was smaller than 0.05 eV Å⁻¹. The potential-alignment, image charge and band-filling corrections were applied by the methodology described in the literatures. ^{86,94,95}

Acknowledgements

This work was funded in part by the Office of Energy Efficiency and Renewable Energy (EERE), U.S. Department of Energy, under Award Number DE-EE0006712, and Ohio Research Scholar Program. This research used the resources of the National Energy Research Scientific Computing Center, which is supported by the Office of Science of the U.S. Department of Energy under Contract No. DE-AC02-05CH11231.

Notes and references

- 1 A. Kojima, K. Teshima, Y. Shirai and T. Miyasaka, *J. Am. Chem. Soc.*, 2009, **131**, 6050–6051.
- National Renewable Energy Laboratory (NREL), http://www.nrel.gov/ncpv/images/efficiency_chart.jpg, accessed August 12, 2016.
- H. Zhou, Q. Chen, G. Li, S. Luo, T. -b. Song, H.-S. Duan, Z.
 Hong, J. You, Y. Liu and Y. Yang, *Science*, 2014, 345, 542–546.
- 4 N. J. Jeon, J. H. Noh, W. S. Yang, Y. C. Kim, S. Ryu, J. Seo and S. Il Seok, *Nature*, 2015, **517**, 476–480.
- W. S. Yang, J. H. Noh, N. J. Jeon, Y. C. Kim, S. Ryu, J. Seo and S. I. Seok, *Science*, 2015, 348, 1234–1237.
- 6 M. Saliba, T. Matsui, K. Domanski, J.-Y. Seo, A. Ummadisingu, S. M. Zakeeruddin, J.-P. Correa-Baena, W. R. Tress, A. Abate, A. Hagfeldt and M. Gratzel, *Science*, 2016, 354, 206–209.
- F. Hao, C. C. Stoumpos, D. H. Cao, R. P. H. Chang and M. G. Kanatzidis, *Nat. Photonics*, 2014, **8**, 489–494.
- 8 N. K. Noel, S. D. Stranks, A. Abate, C. Wehrenfennig, S. Guarnera, A.-A. Haghighirad, A. Sadhanala, G. E. Eperon, S. K. Pathak, M. B. Johnston, A. Petrozza, L. M. Herz and H. J. Snaith, *Energy Environ. Sci.*, 2014, **7**, 3061–3068.
- S. J. Lee, S. S. Shin, Y. C. Kim, D. Kim, T. K. Ahn, J. H. Noh, J. Seo and S. Il Seok, J. Am. Chem. Soc., 2016, 138, 3974–3977.
- W. Liao, D. Zhao, Y. Yu, C. R. Grice, C. Wang, A. J. Cimaroli,
 P. Schulz, W. Meng, K. Zhu, R.-G. Xiong and Y. Yan, *Adv. Mater.*, 2016, 28, 9333–9340.
- 11 B.-W. Park, B. Philippe, X. Zhang, H. Rensmo, G. Boschloo and E. M. J. Johansson, *Adv. Mater.*, 2015, **27**, 6806–6813.
- M. Lyu, J.-H. Yun, M. Cai, Y. Jiao, P. V. Bernhardt, M. Zhang, Q. Wang, A. Du, H. Wang, G. Liu and L. Wang, *Nano Res.*,

- 2016, **9**, 692–702.
- S. Sun, S. Tominaka, J.-H. Lee, F. Xie, P. D. Bristowe and A.
 K. Cheetham, *APL Mater.*, 2016, 4, 31101.
- 14 A. J. Lehner, D. H. Fabini, H. A. Evans, C.-A. Hébert, S. R. Smock, J. Hu, H. Wang, J. W. Zwanziger, M. L. Chabinyc and R. Seshadri, *Chem. Mater.*, 2015, 27, 7137–7148.
- A. H. Slavney, T. Hu, A. M. Lindenberg and H. I. Karunadasa,
 J. Am. Chem. Soc., 2016, 138, 2138–2141.
- A. E. Maughan, A. M. Ganose, M. M. Bordelon, E. M. Miller,
 D. O. Scanlon and J. R. Neilson, *J. Am. Chem. Soc.*, 2016,
 138, 8453–8464.
- W. Meng, B. Saparov, F. Hong, J. Wang, D. B. Mitzi and Y. Yan, Chem. Mater., 2016, 28, 821–829.
- F. Hong, B. Saparov, W. Meng, Z. Xiao, D. B. Mitzi and Y.
 Yan, J. Phys. Chem. C, 2016, 120, 6435–6441.
- 19 B. Saparov, J.-P. Sun, W. Meng, Z. Xiao, H.-S. Duan, O. Gunawan, D. Shin, I. G. Hill, Y. Yan and D. B. Mitzi, *Chem. Mater.*, 2016, **28**, 2315–2322.
- W. J. Yin, T. Shi and Y. Yan, Adv. Mater., 2014, 26, 4653–4658.
- 21 W.-J. W. Yin, J.-H. J. Yang, J. Kang, Y. Yan and S.-H. Wei, *J. Mater. Chem. A*, 2015, **3**, 8926–8942.
- 22 W.-J. Yin, T. Shi and Y. Yan, J. Phys. Chem. C, 2015, 119, 5253–5264.
- 23 A. M. Ganose, C. N. Savory and D. O. Scanlon, *Chem. Commun.*, 2016.
- 24 B. Saparov and D. B. Mitzi, *Chem. Rev.*, 2016, **116**, 4558–4596.
- 25 C. C. Stoumpos, C. D. Malliakas and M. G. Kanatzidis, *Inorg. Chem.*, 2013, **52**, 9019–9038.
- J. Zhang, C. Yu, L. Wang, Y. Li, Y. Ren and K. Shum, *Sci. Rep.*,
 2014, 4, 6954.
- 27 B. Lee, C. C. Stoumpos, N. Zhou, F. Hao, C. Malliakas, C.-Y. Yeh, T. J. Marks, M. G. Kanatzidis and R. P. H. Chang, *J. Am. Chem. Soc.*, 2014, **136**, 15379–15385.
- 28 B. Saparov, F. Hong, J.-P. Sun, H.-S. Duan, W. Meng, S. Cameron, I. G. Hill, Y. Yan and D. B. Mitzi, *Chem. Mater.*, 2015, **27**, 5622–5632.
- 29 P. C. Harikesh, H. K. Mulmudi, B. Ghosh, T. W. Goh, Y. T. Teng, K. Thirumal, M. Lockrey, K. Weber, T. M. Koh, S. Li, S. Mhaisalkar and N. Mathews, *Chem. Mater.*, 2016, acs.chemmater.6b03310.
- J.-C. Hebig, I. Kühn, J. Flohre and T. Kirchartz, ACS Energy Lett., 2016, 1, 309–314.
- 31 E. T. McClure, M. R. Ball, W. Windl and P. M. Woodward, *Chem. Mater.*, 2016, **28**, 1348–1354.
- 32 F. Wei, Z. Deng, S. Sun, F. Xie, G. Kieslich, D. M. Evans, M. A. Carpenter, P. D. Bristowe and A. K. Cheetham, *Mater. Horiz.*, 2016, **3**, 328–332.
- Z. Deng, F. Wei, S. Sun, G. Kieslich, A. K. Cheetham and P.
 D. Bristowe, J. Mater. Chem. A, 2016, 4, 12025–12029.
- 34 Y. Kim, Z. Yang, A. Jain, O. Voznyy, G. Kim, M. Liu, L. N. Quan, F. P. García de Arquer, R. Comin, J. Z. Fan and E. H. Sargent, *Angew. Chemie Int. Ed.*, 2016, **55**, 9586–9590.
- 35 Z. Xiao, W. Meng, D. B. Mitzi and Y. Yan, J. Phys. Chem. Lett., 2016, 7, 3903–3907.
- 36 S. Öz, J.-C. Hebig, E. Jung, T. Singh, A. Lepcha, S. Olthof, F.

- Jan, Y. Gao, R. German, P. H. M. van Loosdrecht, K. Meerholz, T. Kirchartz and S. Mathur, *Sol. Energy Mater. Sol. Cells*, 2016, **158**, 195–201.
- I. C. Smith, E. T. Hoke, D. Solis-Ibarra, M. D. McGehee and
 H. I. Karunadasa, *Angew. Chemie*, 2014, 126, 11414–11417.
- 38 A. H. Slavney, R. W. Smaha, I. C. Smith, A. Jaffe, D. Umeyama and H. I. Karunadasa, *Inorg. Chem.*, 2016, acs.inorgchem.6b01336.
- 39 D. B. Mitzi, in *Progress in Inorganic Chemistry*, 1999, pp. 1–121
- 40 D. B. Mitzi, J. Chem. Soc. Dalt. Trans., 2001, 1–12.
- 41 J. L. Knutson, J. D. Martin and D. B. Mitzi, *Inorg. Chem.*, 2005, **44**, 4699–4705.
- 42 T. Ishihara, J. Lumin., 1994, **60–61**, 269–274.
- 43 K. Tanaka and T. Kondo, *Sci. Technol. Adv. Mater.*, 2003, **4**, 599–604.
- 44 G. C. Papavassiliou, *Mol. Cryst. Liq. Cryst. Sci. Technol. Sect. A. Mol. Cryst. Liq. Cryst.*, 1996, **286**, 231–238.
- 45 T. Ishihara, J. Takahashi and T. Goto, *Phys. Rev. B*, 1990, **42**, 11099–11107.
- Z. Xiao, W. Meng, B. Saparov, H.-S. Duan, C. Wang, C. Feng, W.-Q. Liao, W. Ke, D. Zhao, J. Wang, D. B. Mitzi and Y. Yan, *J. Phys. Chem. Lett.*, 2016, 7, 1213–1218.
- 47 D. Umeyama, Y. Lin and H. I. Karunadasa, *Chem. Mater.*, 2016, **28**, 3241–3244.
- 48 L. N. Quan, M. Yuan, R. Comin, O. Voznyy, E. M. Beauregard, S. Hoogland, A. Buin, A. R. Kirmani, K. Zhao, A. Amassian, D. H. Kim and E. H. Sargent, *J. Am. Chem. Soc.*, 2016, **138**, 2649–2655.
- 49 C. C. Stoumpos, D. H. Cao, D. J. Clark, J. Young, J. M. Rondinelli, J. I. Jang, J. T. Hupp and M. G. Kanatzidis, *Chem. Mater.*, 2016, **28**, 2852–2867.
- D. H. Cao, C. C. Stoumpos, O. K. Farha, J. T. Hupp and M. G.
 Kanatzidis, J. Am. Chem. Soc., 2015, 137, 7843–7850.
- 51 I. B. Koutselas, D. B. Mitzi, G. C. Papavassiliou, G. J. Papaioannou and H. Krautscheid, *Synth. Met.*, 1997, **86**, 2171–2172.
- 52 O. N. Yunakova, V. K. Miloslavskii and E. N. Kovalenko, *Opt. Spectrosc.*, 2012, **112**, 91–96.
- 53 G. C. Papavassiliou, I. B. Koutselas, A. Terzis and M.-H. Whangbo, *Solid State Commun.*, 1994, **91**, 695–698.
- 54 M. Abulikemu, S. Ould-Chikh, X. Miao, E. Alarousu, M. banavoth, G. O. Ngongang Ndjawa, J. Barbé, A. El Labban, A. Amassian and S. Del Gobbo, J. Mater. Chem. A, 2016, 12504–12515.
- 55 M. Vigneshwaran, T. Ohta, S. Iikubo, G. Kapil, T. S. Ripolles, Y. Ogomi, T. Ma, S. S. Pandey, Q. Shen, T. Toyoda, K. Yoshino, T. Minemoto and S. Hayase, *Chem. Mater.*, 2016, acs.chemmater.6b02315.
- 56 R. L. Z. Hoye, R. E. Brandt, A. Osherov, V. Stevanović, S. D. Stranks, M. W. B. Wilson, H. Kim, A. J. Akey, J. D. Perkins, R. C. Kurchin, J. R. Poindexter, E. N. Wang, M. G. Bawendi, V. Bulović and T. Buonassisi, *Chem. A Eur. J.*, 2016, 22, 2605–2610.
- 57 K. Eckhardt, V. Bon, J. Getzschmann, J. Grothe, F. M. Wisser and S. Kaskel, *Chem. Commun.*, 2016, **52**, 3058–3060.
- 58 V. F. Machulin, *Low Temp. Phys.*, 2004, **30**, 964.

- 59 P. Umari, E. Mosconi and F. De Angelis, Sci. Rep., 2014, 4, 4467.
- 60 W.-J. Yin, T. Shi and Y. Yan, *Appl. Phys. Lett.*, 2014, **104**, 63903
- 61 T. Umebayashi, K. Asai, T. Kondo and A. Nakao, *Phys. Rev. B*, 2003, **67**, 155405.
- 62 M. E. Kamminga, H.-H. Fang, M. R. Filip, F. Giustino, J. Baas, G. R. Blake, M. A. Loi and T. T. M. Palstra, *Chem. Mater.*, 2016, 28, 4554–4562.
- 63 Z. Xiao, W. Meng, J. Wang and Y. Yan, *Phys. Chem. Chem. Phys.*, 2016, **18**, 25786–25790.
- 64 D. M. Trots and S. V. Myagkota, J. Phys. Chem. Solids, 2008, 69, 2520–2526.
- 65 S. K. Yeh, S. Y. Wu, C. S. Lee and Y. Wang, *Acta Crystallogr. Sect. B Struct. Sci.*, 1993, **49**, 806–811.
- 66 C. P. Raptopoulou, A. Terzis, G. A. Mousdis and G. C. Papavassiliou, *Zeitschrift für Naturforsch. B*, 2002, 57, 645.
- 67 C. K. Moller, K. Danske Vidensk. Selsk. Mat. Meddelelser, 1960, **32**, 1–13.
- 68 L. Mao, H. Tsai, W. Nie, L. Ma, J. Im, C. C. Stoumpos, C. D. Malliakas, F. Hao, M. R. Wasielewski, A. D. Mohite and M. G. Kanatzidis, *Chem. Mater.*, 2016, 28, 7781–7792.
- M. Safdari, P. H. Svensson, M. T. Hoang, I. Oh, L. Kloo and J.
 M. Gardner, J. Mater. Chem. A, 2016, 4, 15638–15646.
- 70 J. Liu, J. Shi, D. Li, F. Zhang, X. Li, Y. Xiao and S. Wang, Synth. Met., 2016, 215, 56–63.
- 71 H. Tsai, W. Nie, J.-C. Blancon, C. C. Stoumpos, R. Asadpour, B. Harutyunyan, A. J. Neukirch, R. Verduzco, J. J. Crochet, S. Tretiak, L. Pedesseau, J. Even, M. A. Alam, G. Gupta, J. Lou, P. M. Ajayan, M. J. Bedzyk, M. G. Kanatzidis and A. D. Mohite, *Nature*, 2016, **536**, 312–316.
- 72 D. B. Mitzi, C. D. Dimitrakopoulos and L. L. Kosbar, *Chem. Mater.*, 2001, **13**, 3728–3740.
- 73 K. Tanaka, R. Ozawa, T. Umebayashi, K. Asai, K. Ema and T. Kondo, *Phys. E Low-Dimensional Syst. Nanostructures*, 2005, **25**, 378–383.
- 74 T. Baikie, Y. Fang, J. M. Kadro, M. Schreyer, F. Wei, S. G. Mhaisalkar, M. Graetzel and T. J. White, *J. Mater. Chem. A*, 2013. **1**. 5628.
- 75 J. M. Ball, M. M. Lee, A. Hey and H. J. Snaith, *Energy Environ. Sci.*, 2013, **6**, 1739.
- 76 G. A. Mousdis, V. Gionis, G. C. Papavassiliou, C. P. Raptopoulou and A. Terzis, *J. Mater. Chem.*, 1998, **8**, 2259–2262.
- 77 M. L. Agiorgousis, Y. Sun, H. Zeng and S. Zhang, *J. Am. Chem. Soc.*, 2014, **136**, 14570–14575.
- 78 M.-H. Du, J. Phys. Chem. Lett., 2015, **6**, 1461–1466.
- 79 G. Volonakis, M. R. Filip, A. A. Haghighirad, N. Sakai, B. Wenger, H. J. Snaith and F. Giustino, *J. Phys. Chem. Lett.*, 2016, **7**, 1254–1259.
- M. R. Filip, S. Hillman, A. A. Haghighirad, H. J. Snaith and F. Giustino, *J. Phys. Chem. Lett.*, 2016, 7, 2579–2585.
- 81 Z. Xiao, W. Meng, J. Wang and Y. Yan, *ChemSusChem*, 2016, **9**, 2628–2633.
- 82 C. N. Savory, A. Walsh and D. O. Scanlon, *ACS Energy Lett.*, 2016, acsenergylett.6b00471.
- 83 A. Kaltzoglou, M. Antoniadou, A. G. Kontos, C. C.

- Stoumpos, D. Perganti, E. Siranidi, V. Raptis, K. Trohidou, V. Psycharis, M. G. Kanatzidis and P. Falaras, *J. Phys. Chem. C*, 2016, **120**, 11777–11785.
- 84 X. Qiu, Y. Jiang, H. Zhang, Z. Qiu, S. Yuan, P. Wang and B. Cao, *Phys. status solidi Rapid Res. Lett.*, 2016, **10**, 587–591.
- 85 Z. Xiao, H. Lei, X. Zhang, Y. Zhou, H. Hosono and T. Kamiya, *Bull. Chem. Soc. Jpn.*, 2015, **88**, 1250–1255.
- 86 Z. Xiao, Y. Zhou, H. Hosono and T. Kamiya, *Phys. Chem. Chem. Phys.*, 2015, **17**, 18900–18903.
- 87 X. Qiu, B. Cao, S. Yuan, X. Chen, Z. Qiu, Y. Jiang, Q. Ye, H. Wang, H. Zeng, J. Liu and M. G. Kanatzidis, *Sol. Energy Mater. Sol. Cells*, 2017, **159**, 227–234.
- 88 M. H. Kumar, S. Dharani, W. L. Leong, P. P. Boix, R. R. Prabhakar, T. Baikie, C. Shi, H. Ding, R. Ramesh, M. Asta, M. Graetzel, S. G. Mhaisalkar and N. Mathews, *Adv. Mater.*, 2014, **26**, 7122–7127.
- 89 G. E. Eperon, G. M. Paternò, R. J. Sutton, A. Zampetti, A. A. Haghighirad, F. Cacialli and H. J. Snaith, *J. Mater. Chem. A*, 2015, **3**, 19688–19695.
- 90 R. E. Beal, D. J. Slotcavage, T. Leijtens, A. R. Bowring, R. A. Belisle, W. H. Nguyen, G. F. Burkhard, E. T. Hoke and M. D. McGehee, *J. Phys. Chem. Lett.*, 2016, **7**, 746–751.
- 91 Z. Li, M. Yang, J.-S. Park, S.-H. Wei, J. J. Berry and K. Zhu, *Chem. Mater.*, 2016, **28**, 284–292.
- G. Kresse and J. Furthmüller, *Phys. Rev. B*, 1996, **54**, 11169–11186.
- 93 J. P. Perdew, K. Burke and M. Ernzerhof, *Phys. Rev. Lett.*, 1996, **77**, 3865–3868.
- 94 S. Lany and A. Zunger, *Phys. Rev. B*, 2008, **78**, 235104.
- 95 Z. Xiao, F.-Y. Ran, H. Hosono and T. Kamiya, *Appl. Phys. Lett.*, 2015, **106**, 152103.